Eleventh International Conference on CFD in the Minerals and Process Industries
CSIRO, Melbourne, Australia
7-9 December 2015

STRUCTURE-DEPENDENT DRAG MODEL FOR SIMULATION OF GAS-SOLIDS FLUIDIZED BEDS

Lu HUILIN*, Liu GUODONG, Wang SHUAI and Yu WENHAO

School of Energy Science and Engineering, Harbin Institute of Technology, Harbin, 160001, CHINA

*Corresponding author, E-mail address: huilin@hit.edu.cn

ABSTRACT

Clusters in risers and bubbles in bubbling fluidized bed effect flow behavior and heat and mass transfer in gas-solid fluidized beds. A structure-dependent drag model is proposed to improve drag coefficient predictions for heterogeneous gas-solid flows with clusters in risers and bubbles in bubbling fluidized beds. To model bubbling fluidized beds, the local flow in the grid cell is resolved into three subsystems: the dilute phase that characterizes the bubbles, the dense phase that characterizes the emulsion, and the interphase between dense phase and dilute phase. In a riser, particle movements are in the form of clusters in the dense phase or in the form of a dispersed particle in the dilute phase in the grid cell. A micro-meso-grid scales equation set consists of six hydrodynamic equations and one stability criteria with bivariate extreme value theory as a function of eight independent variables and four dependent parameters on the basis of four grid parameters of velocity of gas and solids phases, volume fraction of gas phase and gas pressure gradient. The structure-dependent drag model is verified by CFD simulations by coupling with the two-fluid model in gas-solids fluidized beds. The distributions of velocity and volume fraction of clusters, and cluster diameters in a riser and the profiles of velocity and diameter of bubbles in a gas-solids bubbling fluidize bed are predicted. The simulated results are compared with experimental data.

INTRODUCTION

The clustering of particles in risers and bubbles in bubbling fluidized beds continue to be a fundamental issue in hydrodynamics of dense gas-solids flow. Experiments show that particle clusters and gas bubbles are existed in gas-solids fluidized beds. The formations of clusters and bubbles depend on operating conditions and material properties. In the case of circulating fluidized beds with Geldart Group A powders, the forces or possible interactions responsible for particle clustering include hydrodynamics (drag minimization), inelastic collisions, electrostatic charging, capillary and van der Waals forces. However, no one force may be responsible for all types of particle clustering and gas bubbles. It is more likely that several forces may play roles of varying magnitudes depending on the particles properties and local environments including velocity, solids volume fraction and fluid pressure.

Computational fluid dynamics (CFD) is an effective tool for understanding the fundamental hydrodynamics of gas and particles in fluidized beds. However, a major challenge for CFD models is to realistically resolve the effect of clusters of bubbles on the momentum exchange between the gas phase and solids phase. Generally, the drag force acting on particles is represented by the product of the drag coefficient βgs and the slip velocity between the two phases. To date, several drag models have been developed to predict the interphase drag coefficient. A comparison of predicted drag coefficient using O'Brien and Syamlal drag model and Huilin-Gidaspow drag model (2012) is shown in Figure 1 as a function of solids volume fraction. It clear shows the clusters contribution on drag in gas-solids flow system. O'Brien and Syamlal drag model was limited to only two solid mass fluxes due to an empirical factor. The energy minimization multiscale approach (EMMS) developed by Li et al. (1999) has been used to predict steady flow in circulating fluidized beds. However, the validation of EMMS drag model is still a problem because the model equations stem from a global fluidized bed system, not for grid cells of numerical simulations. Also the equation for predicting cluster diameter is not valid to use in the counter-current flow with gas flow-up and clusters flow-down. On the other hand, the filtered drag models proposed by Sundaresan group (2011) and Simonin group (2013) are obtained using finely resolved simulations as the computational grid is refined and more flow structures are resolved. These filtered models are the analogue of large-eddy simulation of single phase turbulent flow, where one simulates spatial and spatio-temporal patterns occurring at the macro-scale using the conservations of mass and momentum, but accounts for the effects of meso-scale structures occurring at a scale smaller than the grid size through additional closure relations.

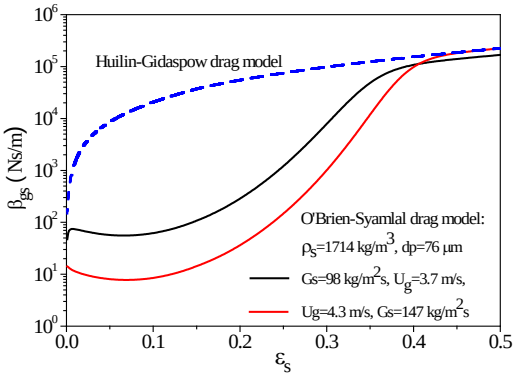

Figure 1: Predicted drag by Huilin-Gidaspow and O'Brien-Syamlal drag models.

CLUSTER STRUCTURE-DEPENDENT (CSD) DRAG MODEL IN RISERS

In the present work, an Eulerian multi-fluid model, which considers the conservation of mass and momentum for the solid and gas phases, has been adopted. The kinetic theory of granular flow, which considers the conservation of solid fluctuation energy, has been used for closure.

Figure 2 shows the flow structure of particles in a grid cell which means particle movement is in the form of clusters in the dense phase or in the form of a dispersed particle in the dilute phase. This structure is described by eight independent variables. That is, gas volume fractions of the dilute phase and the dense phase (ε_{dil}, ε_{den}), gas superficial velocity of the dilute and the dense phases ($U_{g,dil}$, $U_{g,den}$), superficial velocity of particles in the dilute phase and the dense phase ($U_{s,dil}$, $U_{s,den}$), cluster size (dc) and volume fraction of dense phase (f). The parameters of a grid cell are velocities of gas and solids phases, gas volume fraction and gas pressure gradient along flow direction u_g, u_s, ε_g and $\partial p/\partial y$) from TFM. The mathematical model to describe flow behavior of gas and particles can be formulated as the following set of non-linear equations.

1. Momentum equation for clusters in the dense phase along flow direction

For simplicity, we assume that the stress tensor of dense phase is neglected. From the clusters momentum equation of dense phase along flow direction at the steady state is

$$n_{den}F_{den} + n_{\text{int}}F_{\text{int}} = f(1-\varepsilon_{den})(\rho_s - \rho_g)(g + a_{s,den}) + f(1-\varepsilon_{den})\frac{\partial p}{\partial y} \quad (1)$$

$$a_{s,den} = \frac{\partial}{\partial y}\left[\frac{fU_{s,den}}{(1-\varepsilon_{den})}\frac{fU_{s,den}}{(1-\varepsilon_{den})}\right] \quad (1a)$$

2. Momentum equation for dispersed particles in the dilute phase along flow direction

If the stress tensor of dilute phase is negligible at the steady state, the dispersed particles momentum equation of dilute phase along flow direction at the steady state is

$$n_{dil}F_{dil} = (1-f)(1-\varepsilon_{dil})(\rho_s - \rho_g)(g + a_{s.dil}) + (1-f)(1-\varepsilon_{dil})\frac{\partial p}{\partial y} \quad (2)$$

$$a_{s.dil} = \frac{\partial}{\partial y}\left[\frac{(1-f)U_{s,dil}}{(1-\varepsilon_{dil})}\frac{(1-f)U_{s,dil}}{(1-\varepsilon_{dil})}\right] \quad (2a)$$

3. Momentum equation for gas phase in the dilute and dense phases along flow direction

The gas stress tensors of dense phase and dilute phase are also assumed to be neglected. The gas gravitational forces of the dilute phase and dense phase are negligible because of small gas density. The gas momentum equation of the dilute and dense phases is:

$$\frac{n_{den}F_{den}}{f\varepsilon_{den}} = \frac{n_{dil}F_{dil}}{(1-f)\varepsilon_{dil}} + \frac{n_{\text{int}}F_{\text{int}}}{(1-f)\varepsilon_{dil}} + \rho_g(a_{g.dil} - a_{g.den}) \quad (3)$$

$$a_{g.dil} = \frac{\partial}{\partial y}\left[\frac{(1-f)U_{g,dil}}{\varepsilon_{dil}}\frac{(1-f)U_{g,dil}}{\varepsilon_{dil}}\right]$$

and

$$a_{g.den} = \frac{\partial}{\partial y}\left[\frac{fU_{g,den}}{\varepsilon_{den}}\frac{fU_{g,den}}{\varepsilon_{den}}\right] \quad (3a)$$

4. Mass balance of gas phase

From the gas mass balance of dense phase and dilute phase, the velocity of gas phase in the cell is expressed as:

$$u_g = \frac{1}{\varepsilon_g}\left[fU_{g,den} + (1-f)U_{g,dil}\right] \quad (4)$$

5. Mass balance of solids phase

From the mass balance of particles in the dense phase and dilute phase, the velocity of particles in the cell is expressed as:

$$u_s = \frac{1}{(1-\varepsilon_g)}\left[fU_{s,den} + (1-f)U_{s,dil}\right] \quad (5)$$

6. Overall gas volume fraction

$$\varepsilon_g = f\varepsilon_{den} + (1-f)\varepsilon_{dil} \quad (6)$$

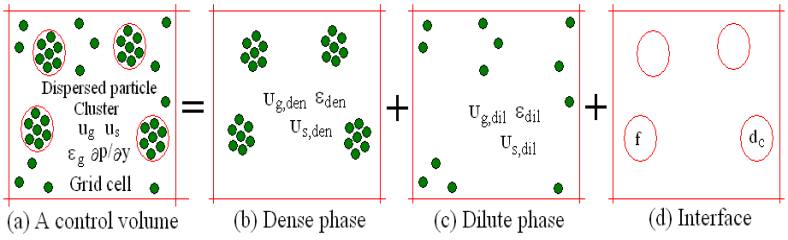

Figure 2: Flow structure of clusters and dispersed particles in a grid cell.

7. Stability criterion (minimization of energy dissipation by heterogeneous drag)

The stability condition is expressed as the extremum of energy dissipation by drag per unit mass of particles.

$$N_{df} = \frac{\Omega}{(1-\varepsilon_g)\rho_s} = \frac{1}{(1-\varepsilon_g)\rho_s}\left[n_{den}F_{den}\,U_{g,den} + n_{dil}F_{dil}\,U_{g,dil} + n_{int}F_{int}\,U_{g,dil}(1-f) \rightarrow \text{minimum}\right] \quad (7)$$

8. Bivariate extreme value (BEV) theory

In the bivariate extreme value (BEV) theory, the tail dependence parameters estimate numerically the importance of asymptotic dependence between two variables. The bivariate extreme value distribution can thus be described by a function of just one real variable, the dependence function. Using BEV theory, the stability condition Eq. (7) is expressed by

$$\text{minimize}\left\{\left[N_{df}(U_{g,den}, U_{s,den}, U_{g,dil}, U_{s,dil}, f, d_c)\right] \middle| (\varepsilon_{dil} \in R_1, \varepsilon_{den} \in R_2)\right\} \quad (8)$$

where $\mathbf{R}_1$ and $\mathbf{R}_2$ are the domains of variation of ε_{dil} and ε_{den}.

Thus, a micro-meso-grid scales (M2GS) equation set which comprises six hydrodynamic equations of Eqs. (1)-(6) and a stability condition of Eq. (8) with bivariate extreme value (BEV) theory is closed to solve eight independent variables (ε_{gf}, U_{gf} and U_{sf} for micro-scale. f, ε_{gc}, d_c, U_{gc} and U_{sc} for meso-scale) and four dependent parameters ($a_{g,den}$, $a_{g,dil}$, $a_{s,den}$ and $a_{s,dil}$) on the basis of grid parameters (ε_g, u_s, u_g and dp/dy), seeing in Figure 3. Thus, the heterogeneous drag coefficient β_{gs} is determined.

Simulations are conducted using the CSD drag model and Huilin-Gidaspow drag models and results are compared with the experimental data of Wei et al. (1998) measured in a 30.5 mm vertical pipe using a laser-Doppler velocimeter (LDV). The diameter and density of particles are 54 μm and 1398 kg/m^3, respectively. Figure 4 shows the distribution of drag coefficient as a function of solids volume fraction. Roughly, the drag coefficient predicted by CSD drag model decreases, reaches minimum, and then increases with the increase of solids volume fraction. The drag coefficient by means of Huilin-Gidaspow drag model is also given as a function of solids volume fraction. The difference of drag coefficients between the CSD drag model and Huilin-Gidaspow drag model is obvious. We see that the heterogeneity reduces drag instead of increasing it at the low solids volume fraction. The reason is that when the flow is dilute, the particle collision probability is small, and results in decreased resistance with more gas flow through the dilute phase. So that the dilute phase occupies more space, and there are few opportunities to form clusters and the flow tends to be homogeneous. Gradually, the dense phase is formed as clusters, Huilin-Gidaspow drag model is also given as a function of solids volume fraction.

The difference of drag coefficients between the CSD drag model and Huilin-Gidaspow drag model is obvious. We see that the heterogeneity reduces drag instead of increasing it at the low solids volume fraction. The reason is that when theflow is dilute, the particle collision probability is small, and results in decreased resistance with more gas flow through the dilute phase. So that the dilute phase occupies more space, and there are few opportunities to form clusters and the flow tends to be homogeneous. Gradually, the dense phase is formed as clusters, which act as large particles with the increase of solids volume fraction. The drag then decreases more rapidly than with the homogeneous drag. When the flow is dense, the particles tend to form clusters due to the large collision probability. As a result, the drag reaches a minimum. As the solids volume fraction increases beyond some critical value, the interaction between the dense phase and the dilute phase increases. Therefore, clusters can only form within a certain range of conditions. As the cluster effect disappears, the drag coefficient again approximates the homogeneous case predicted by means of Huilin-Gidaspow drag model.

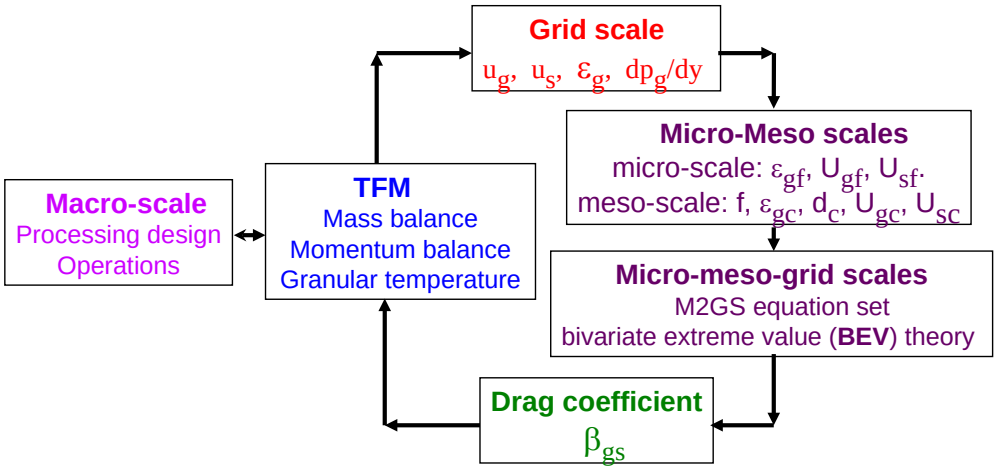

Figure 3: CSD drag coefficient using M2GS model with BEV

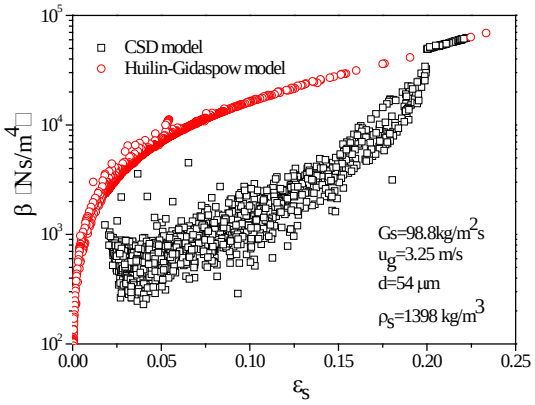

Figure 4: Drag coefficient as a function of solids volume fraction

Figure 5 shows the distribution of predicted cluster diameter as a function of solids volume fraction. Roughly, the predicted cluster diameters increase, reach maximum, and then decrease with the increase of solids volume fractions. As the amount of solids increases, particles tend to aggregate to achieve less resistance. This leads in general to larger diameter, and until the cluster size reaches a turning point. Beyond this turning point, the cluster diameters decrease, hinting at a possible change in the flow patterns over the region originally thought to be completely homogeneous. Harris et al. (2002) presented correlations for predicting the properties of cluster of particles traveling near the riser wall. The cluster sizes in experimental investigations usually refer to the mean vertical cluster length because of the considerable variation of cluster shapes. Thus, more attention should be paid to the physical definition when employing a cluster diameter correlation.

This indicates the cluster diameter correlation has significant effect on the hydrodynamics predictions and should be selected carefully for the prevailing flow conditions.

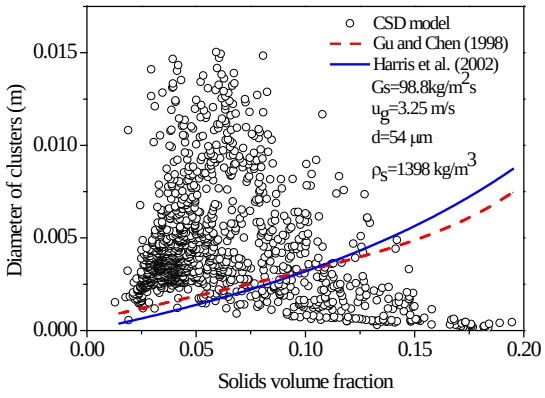

Figure 5: Cluster diameter as a function of solids volume fraction

Figure 6 shows the profile of predicted volume fraction of dense phase (f) and solids volume fraction of clusters ($\varepsilon_{s,den}$) as a function of solids volume fraction. Generally speaking, the predicted volume fractions of dense phase, f, increase, reach maximum, and then decrease with the increase of solids volume fraction. The solids volume fraction of clusters defines the ratio of the volume of particles in the clusters to the volume of dense phase of the grid cell. The high value of the solids volume fraction of clusters represents more particles within the cluster. We see that the clusters are dense with the increase of solids volume fraction. The calculated solids volume fraction of clusters using the correlation proposed by Gu and Chen (1998) is given as a function of solids volume fraction. Both numerical simulations and correlation give the solids volume fractions of dense phase increase with the increase of solids volume fraction. However, the difference between them is obvious. Examination of the correlation proposed by Harris et al (2002) concerning solids volume fraction of clusters suggests that the volume fraction of cluster requires the local instantaneous solid concentration greater than the time-mean solid concentration by at least n times the standard deviation. A cluster would thus be identified if the instantaneous solid concentration exceeds this threshold.

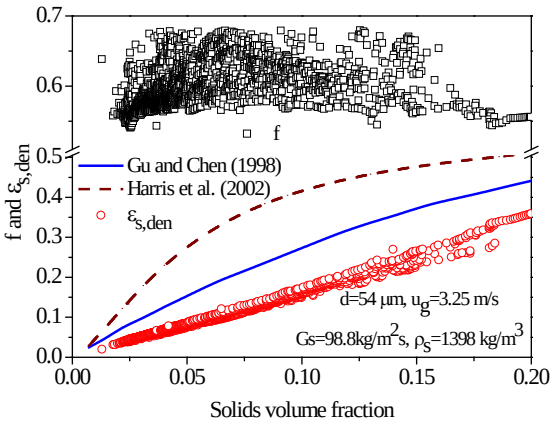

Figure 6: Volume fraction of dense phase and solids volume fraction of clusters

Figure 7 shows a comparison of experimental and computed solids volume fraction profiles at two heights. Both drag models give a high solids volume fraction near the walls, and a low volume fraction of particles at the center regime. Comparing to simulations by means of Huilin-Gidaspow drag model, the predictions using CSD drag model give a reasonable quantitative agreement with experiments. The predictions by means of CSD drag model show a profile of the experimental data more accurately than those using Huilin-Gidaspow drag model at height of 3.92 m. At 6.26 m height, the simulation using Huilin-Gidaspow drag model gives a reasonable qualitative and quantitative agreement with the experimental data at

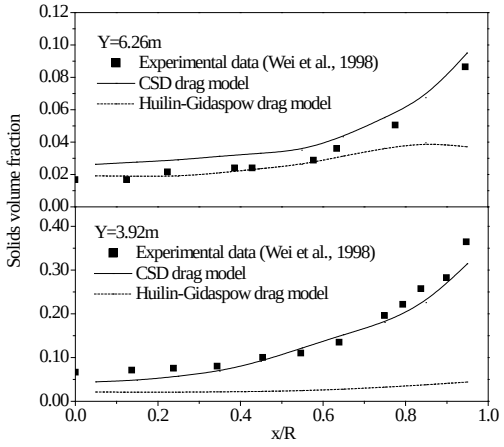

Figure 7: Experimental and computed solids volume fractions

the center regime of the riser. However, near the wall, only the CSD drag model shows a quantitative agreement with the experimental data, whereas, the Huilin-Gidaspow drag model shows wide discrepancies.

BUBBLE-STRUCTURE-DEPENDENT (BSD) DRAG MODEL AND SIMULATIONS OF BUBBLING FLUIDIZED BEDS

To model bubbling fluidized beds, the local flow in the grid cell is resolved into three subsystems: the dilute phase that characterizes the bubbles, the dense phase that characterizes the emulsion, and the interphase between dense phase and dilute phase, as is displayed in Figure 8. For the dense phase and dilute phase, gas and particles are accelerated or decelerated by complex interactions. Such structure is described by six independent variables. That is, gas volume fractions of the bubble phase and the emulsion phase (ε_b, ε_e), gas superficial velocity of the emulsion and the bubble phases ($U_{g,e}$, U_b), superficial velocity of particles in the emulsion phase ($U_{s,e}$), bubble size (d_b) and volume fraction of bubble phase (b). Here, as a first approximation, particles in the bubble phase is assumed negligible, so, ε_b = 1.0. These six parameters depends on velocities of gas and solids phases, gas volume fraction and gas pressure gradient along flow direction (u_g, u_s, ε_g and $\partial p/\partial y$) of a grid cell.

1. Momentum equation of particles in emulsion phase along flow direction

The momentum equation of particles in emulsion phase along flow direction at the steady state is

$$n_e F_{de} + n_b F_{db} = (1-\delta_b)(1-\varepsilon_e)\nabla p + (1-\delta_b)(1-\varepsilon_e)(\rho_s - \rho_p)(\mathrm{g} + \mathrm{a}_{s,e}) + \nabla p_s \quad (9)$$

where p_s is the normal force due to the collisions of particles which is predicted by the modulus of particles compressibility. F_{de} and F_{db} are the drag forces between gas phase and particles, and interphase interactions between bubble and particles. $a_{s,e}$ is the acceleration of particles in the emulsion phase.

2. Momentum equation of gas phase in emulsion phase and bubble phase along flow direction

The momentum equation of gas phase in bubble phase along flow direction at the steady state is

$$n_b F_{db} = -\delta_b \nabla p - \nabla p_b - \delta_b \rho_p (\mathrm{g} + a_{g,b}) \quad (10)$$

where F_{db} is the drag forces of bubbles. $a_{g,b}$ is the acceleration of bubbles.

The momentum equation of gas phase in emulsion phase along flow direction at the steady state is

$$n_e F_{de} = -(1-\delta_b)\varepsilon_e \nabla p - (1-\delta_b)\varepsilon_e \rho_p (\mathrm{g} + a_{g,e}) \quad (11)$$

where F_{db} is the drag forces of bubbles. $a_{g,e}$ is the acceleration of gas phase in the emulsion phase. Combining Eq. (10) and (11), it gives a momentum equation of gas phase in a gird cell.

$$\frac{\delta_b}{(1-\delta_b)\varepsilon_e} n_e F_{de} = n_b F_{db} - \delta_b \rho_g (a_{g,e} - a_{g,b}) + \nabla p_b \quad (12)$$

3. Mass balance of gas phase

From the gas mass balance of emulsion phase and bubble phase, the velocity of gas phase in the cell is expressed as:

$$u_g = \frac{\left[(1-\delta_b)U_{g.e} + \delta_b U_b\right]}{\varepsilon_g} \quad (13)$$

4. Mass balance of solids phase

From the mass balance of particles in the emulsion phase and bubble phase in which without particles, the velocity of particles in the cell is expressed as:

$$u_s = \frac{(1-\delta_b)}{(1-\varepsilon_g)} U_{s.e} \quad (14)$$

5. Overall gas volume fraction

$$\varepsilon_g = f\,\varepsilon_{den} + (1-f)\varepsilon_{dil} \quad (15)$$

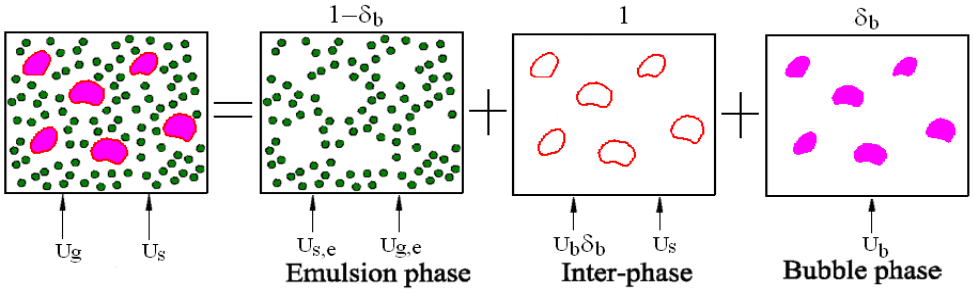

Figure 8: Flow structure of bubbles and emulsion phase in a grid cell

6. Stability criterion (minimization of energy dissipation by heterogeneous drag)

The stability condition of gas and bubbles is expressed as the extremum of energy dissipation by drag per unit mass of particles.

$$N_{df} = \frac{1}{(1-\varepsilon_g)\rho_s}[n_e F_{de} U_{g,e} + n_b F_{db} U_b \delta_b] \rightarrow \text{minimum} \quad (16)$$

Thus, a micro-meso-grid scales (M2GS) equation set which comprises five hydrodynamic equations of Eqs. (9), (12), (13)-(15) and a stability condition of Eq. (16) is closed to solve six independent variables (ε_e, $U_{g,e}$ and $U_{s,e}$ for micro-scale. δ_b, d_b and U_b for meso-scale) on the basis of grid parameters (ε_g, u_s, u_g and $\partial p/\partial y$). Thus, the bubble-structure-dependent (BSD) drag coefficient β_{BSD} is determined.

$$\beta_{BSD} = \frac{(1-\varepsilon_s)}{U_{slip}}\left[n_e F_{de} + n_b F_{db}\right] \quad (17)$$

Hence, three dependent parameters of accelerations ($a_{g,e}$, $a_{s,e}$ and $a_{g,b}$) are also calculated from six independent variables. Figure 9 shows the drag coefficients predicted by BSD drag coefficient and Gidaspow drag model as a function of solids volume fractions in a gas-particles bubbling fluidized bed. Both drag coefficients are increased with the increase of solids volume fractions. We also find that drag coefficient predicted by Gidaspow drag model is larger than that predicted by BSD drag coefficient model.

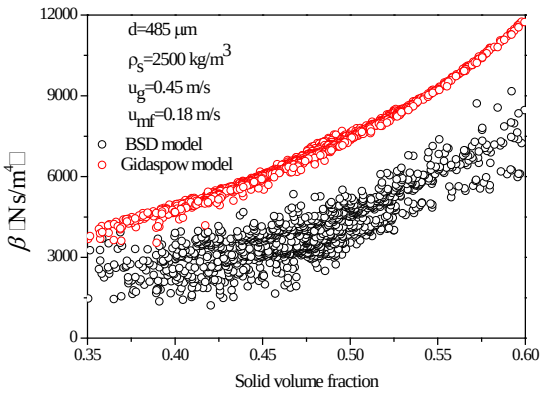

Figure 9: Profile drag coefficients as a function of solids volume fractions

Figure 10 shows the contour plot of an instantaneous solid volume fraction obtained by simulation and experimental data measured by an electrical capacitance tomography (ECT) sensor at the inlet superficial gas velocity of 0.55 m/s. It can be observed that the model prediction can capture a distribution similar to that of the measured result. There is an accumulation of particles toward the walls owing to the wall friction. The motion of bubbles in the center leads to a lower solid volume fraction. In comparison to the solid distribution at low velocity, a high inlet velocity enhances the lateral discrepancy of the solids volume fractions. Figure 11 shows the solids volume fractions are low in the center regime and increases toward the wall. The BSD drag model can obtain a fair prediction with experimental data. The traditional Gidaspow drag model under predicts the solids volume fractions, which is related to the overlook of the mesoscale structure effect. The prediction by BSD drag model can agree reasonably with the experimental data using coarse-grid resolution. From the profiles of solid volume fractions, a higher operating velocity results in a significant lateral discrepancy in the solid distribution.

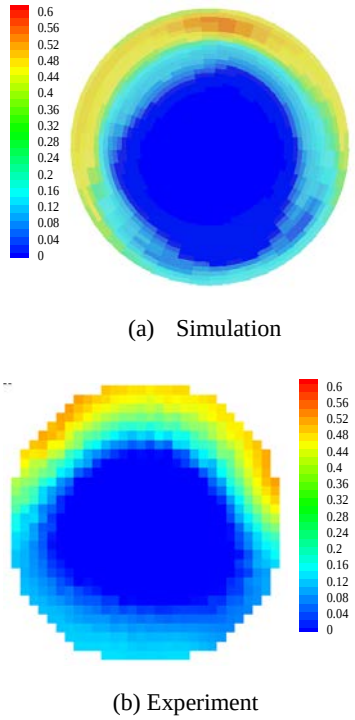

(a) Simulation

(b) Experiment

Figure 10: Comparisons of simulated results (a) and measured data (b) in a bubbling fluidized bed

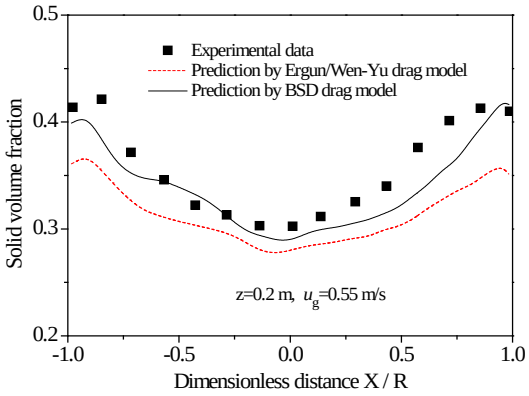

Figure 11: Profile of measured and simulated solids volume fractions

4. CONCLUSION

The present CSD drag model is solved by means of a micro-meso-grid scales (M2GS) equation set which consists of six hydrodynamic equations and one stability criteria with bivariate extreme value (BEV) theory as a function of eight independent variables ($U_{g,den}$, $U_{s,den}$, $U_{g,dil}$, $U_{s,dil}$, $\varepsilon_{g,dil}$, $\varepsilon_{g,den}$, f and d_c) and four dependent parameters ($a_{s,den}$, $a_{g,den}$, $a_{s,dil}$ and $a_{g,dil}$) describing flow of micro-scale of dispersed particles and meso-scale of clusters on the

basis of grid parameters (ε_g, u_s, u_g and $\partial p/\partial y$). Predictions using CSD drag model show reasonable quantitative agreement with the experimental data.

A BSD drag coefficient model is developed to account for the effect of bubbles structure solving six independent variables (ε_e, $U_{g,e}$ and $U_{s,e}$ for micro-scale. δ_b, d_b and U_b for meso-scale) based on the grid parameters (ε_g, u_s, u_g and $\partial p/\partial y$) in bubbling fluidized beds. The effects of solid pressure due to particle-particle collisional interaction and bubble-induced added mass force are evaluated. Predictions using BSD drag model show reasonable quantitative agreement with ECT experimental data.

REFERENCE

AGRAWAL K, LOEZOS PN, SYAMLAL M, SUNDARESAN S., The role of meso-scale structures in rapid gas-solid flows. *J. Fluid Mechanics*, **445**, 151-185, 2011.

ANSYS-Fluent Inc., *Fluent users manual Version 14.0*, New Hampshire, USA, 2012.

HARRIS A.T., DAVIDSON J.F., THORPE R.B., The prediction of particle cluster properties in the near wall region of a vertical riser, Powder Technology, **127**, 128-143, 2002.

GU W.K., CHEN J.C., A model for solid concentration in circulating fluidized beds. In: Fan, L.S., Knowlton, T.M. (Eds.), *Fluidization IX*. Engineering Foundation, Durago, Colorado, 501-508, 1998.

LI J., CHEN C.L., ZHANG Z.D., YUAN J., NEMET A., FETT F. N., The EMMS model-its application, development and updated concepts. *Chem. Eng. Sci*. **54**, 5409- 5425, 1999.

O'BRIEN T.J., SYAMLAL M., Particle cluster effects in the numerical simulation of a circulating fluidized bed, *4th International Conference on CFB*, Somerset, USA, 430-443, 1993.

PARMENTIER J.F., SIMONIN O., DELSART O., A functional subgrid drift velocity model for filtered drag prediction in dense fluidized bed. *AIChE J*., **58**, 1084-1098, 2012.

SHUAI W., GUANGBO Z., GUODONG L., HUILIN L., FEIXIANG Z., Hydrodynamics of gas-solid risers using cluster structure-dependent drag model, *Powder Technology*, **254**, 214-227,2014

SHUAI W., HUANG L., JIANMIN G., HUILIN L., GUODONG L., PENGFEI X. CFD simulation of gas-solid flow with a cluster structure-dependent drag coefficient model in circulating fluidized beds, *Applied Mathematical Modelling*, **37**, 8179-8202, 2013

WEI F., LIN H., CHENG Y., WANG Z., JIN Y., Profiles of particle velocity and solids fraction in a high-density riser. *Powder Technology*, **100**, 183-189, 1998.